Two-scale approach to dynamic localization failure of AISI 316H stainless steel sheets

W.Gambin [*]   K.Kowalczyk-Gajewska [†]

L.T.Kudrjavceva [‡]   M.V.Micunovic [§]

Abstract

Dynamic localization failure of a thin sheet made of AISI 316H steel is considered on the macroscopic and mesoscopic level for proportional and nonproportional stress paths. On the macroscopic level, we propose: (1) the replacement of time as independent variable by a function of plastic dissipation and (2) dependence of the initial equivalent yield stress on stress rate. On the mesoscopic level - the regularized Schmid model for description of the single grain behaviour is used and the polycrystalline yield surface generated by the texture development enables to improve the Forming Limit Diagrams for the sheet element.

Key words: dynamic localization failure, Forming Limit Diagrams, regularized Schmid law, sheet textures

1 Introduction

Increasing rate of metal forming processes requires a new approach to the problem of necking failure in sheet metals. During dynamic localization failures two problems appear: choice of proper constitutive description of the macroscopic sheet element, and analysis of the necking on the mesoscopic - polycrystalline level.

[*]Faculty of Mechatronics, Warsaw University of Technology

[†]Institute of Fundamental Technological Research, Polish Academy of Sciences, Warsaw, Poland

[‡]Faculty of Mechanical Engineering, Kragujevac University - Kragujevac, Serbia

[§]Faculty of Mechanical Engineering, Kragujevac University - Kragujevac, Serbia, e-mail: mmicun@EUnet.yu

On the macroscopic level, two constitutive models describing the dynamic behaviour of viscoplastic material are proposed: a modification of the Perzyna-Chaboche-Rabotnov (PCR) model [1, 2, 3] and the Micunovic-Albertini-Montagnani (MAM) model (cf. [4]). In both models, evolution equations for the plastic strain rate tensor are endochronic permitting scaling of plastic strain rate. The models are calibrated for a large range of strain rates and different multi-axial strain histories of AISI 316H [5]. In the presented paper, these new models are applied to two typical ranges of strain rate: a) "low strain rate" ($\sim 10^{-3}$ [s^{-1}]) corresponding to stress rate ~ 15 [MPa·s^{-1}] and b) "medium strain rate" (~ 1 [s^{-1}]) leading to stress rate ~ 1900 [MPa·s^{-1}]. The adequate initial yield stresses are: $Y_0 = 280$ MPa, for the low strain rate, and $Y_0 = 329$ MPa - for the medium strain rate [6]. A sheet failure due to the strain localization is assumed to be induced by a thin shallow groove perpendicular to the first of principal stresses, according to the Marciniak and Kuczyski approach [7]. If we denote by $\bar{\varepsilon}$ the equivalent strain out of the groove, and by $\bar{\varepsilon}_B$ — the equivalent strain in the groove, then according to this approach, the upper bound of instability onset is determined by the condition: $d\bar{\varepsilon}/d\bar{\varepsilon}_B = 0$. Two stress histories defined by a proportional and non-proportional paths are investigated using the modified PCR-model and MAM-model.

On the mesoscopic level, the deformed sheet element is considered as a polycrystalline aggregate. For the description of the single grain behaviour, the regularized Schmid model is used [8, 9, 10]. By analysis of crystallographic lattice reorientations at each grain of the polycrystalline element, the texture development in the groove and outside of the groove is shown. The analysis is performed for different strain paths. It enables to predict an initiation and development of strain localization in the sheet element. Using the polycrystalline yield surface generated by the developed texture [11, 12], one can improve the Forming Limit Diagrams for the sheet, calculated previously on the macroscopic level.

2 Localization according to macroscopic models

2.1 The viscoplasticity models

Consider a sheet element whose original thinning is described by ratio $f_0 = t_B/t_A$ (see figure 2.1). Subscript "B" stands for the quantities in the groove, and subscript "A" - out of the groove. As a measure of plastic strain, Hill's logarithmic tensor ε_P is chosen. So, after strain localization the plastic strain

is described by two tensors ε_P^A and ε_P^B. The quantities S_1 and S_2 at the figure 2.1 are principal components of the second Piola-Kirchhoff stress tensor $\mathbf{S}$. Denote by $\mathbf{S}_D$ its deviatoric part, and by $\mathbf{D}_P$ the corresponding plastic strain tensor. Then, the von Mises equivalent stress and equivalent plastic strain rate are defined as: $\bar{\sigma} = [(3/2)\mathrm{tr}(\mathbf{S}_D^2)]^{1/2}$ and $\dot{\bar{\varepsilon}}_P = [(2/3)\mathrm{tr}(\mathbf{D}_P^2)]^{1/2}$. It is known
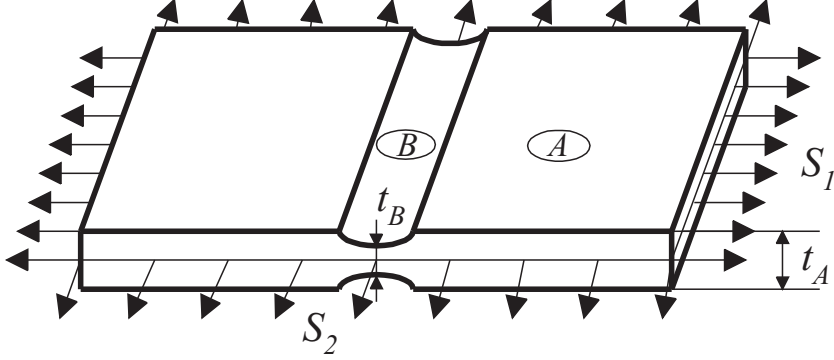

Figure 1: A sheet with initial imperfection

fact that initial yield stress under dynamic loading depends on strain rate or stress rate: at higher stress rates the initial stress yield is larger. On the other hand, the phenomenon of delayed yielding inherent to some metals and alloys is observed [3]: stress under dynamic loading exceeds its static value and plasticity starts after a certain time called delay time. Let plastic deformation commence at time t^*. Denote by Y_0 the initial equivalent static yield stress, and by $Y = Y(\dot{\bar{\sigma}}\,|_{t=t^*})$ — the initial equivalent dynamic yield stress. Then, the accumulated plastic strain is governed by corresponding constitutive equation having the following form [4]:

$$\bar{\varepsilon}_P(t) = \int_0^t J(t-\tau)\,\dot{\bar{\sigma}}(\tau)\,d\tau \qquad \text{and} \qquad \dot{\bar{\varepsilon}}_P(t) = J(0)\dot{\bar{\sigma}}(t), \qquad (1)$$

where $J(t-\tau) = \{0$ if $\tau < t^*$, and $\exp(-M)$ if $\tau \geqslant t^*\}$. Here M is an universal constant for tension and shear at strain rates introduced and determined in [4] for the extremely wide range from $10^{-3}[s^{-1}]$ to $10[s^{-1}]$. The above is used in two alternative types of evolution equations, which are then exploited for a subsequent analysis of localization phenomena.

The first type of evolution equations is proposed in the MAM model. Below, we use a simplified version of the model. Let us introduce the stress tensor invariants: $s_1 = \mathrm{tr}\mathbf{S}$, $s_2 = \mathrm{tr}\mathbf{S}_D^2$. Then, the model is described by the following

tensor representation:

$$\mathbf{D}_{\mathrm{P}} = \Lambda \sum_{\alpha=1}^{2} \Gamma_\alpha(s_1, s_2)\mathbf{H}_\alpha, \tag{2}$$

where

$$\mathbf{H}_1 = \frac{1}{Y_0}\Big[\mathbf{S} - \frac{1}{3}\mathbf{1}tr\mathbf{S}\Big] \equiv \mathbf{S}_D, \qquad \mathbf{H}_2 = \frac{1}{Y_0^2}\Big(\mathbf{S}_D^2\Big)_D,$$

and corresponding scalar coefficients depend on the listed invariants as follows:

$$\Gamma_1 = a_1 + a_2\, s_1 + a_3 s_2, \qquad \Gamma_2 = -\tfrac{3}{2}\, a_2.$$

The scalar coefficient Λ takes the form:

$$\Lambda = \eta\, (\bar{\sigma} - Y)(\frac{\bar{\sigma}}{Y_0} - 1)^\lambda \frac{D\bar{\sigma}}{Dt}\exp(-M). \tag{3}$$

Herein Y is the dynamic initial equivalent yield stress, Y_0 $-$ its static counterpart, $\eta(x)$ - the Heaviside's function, λ - a material constant and M $-$ the above introduced and determined universal viscoplastic material constant. Inserting of (3) into (2) leads to an evolution equation seemingly characteristic for rate independent materials. However, the rate dependence appears in stress rate dependent value of the initial yield stress Y, which has a triggering role for inelasticity onset. The model could be named as "quasi rate independent".

In the similar way the equations (1), (3) are inserted in the paper [4] into the PCR model [1, 2], replacing time as independent variable by the von Mises equivalent stress.

In both cases the obtained evolution equations are endochronic permitting scaling of plastic strain rate. This is useful for calibration in very wide strain rate range from low to almost impact strain rates.

2.2   Localization

The localization instability for the plate is governed by the following 4 differential equations:

$$\frac{d\varepsilon_{Pi}^\alpha}{d\bar{\sigma}^\alpha} = F_i^\alpha(\varepsilon_{P1}^\alpha, \varepsilon_{P2}^\alpha, \sigma_1^\alpha, \sigma_2^\alpha); \alpha = A, B, i = 1, 2, \tag{4}$$

where, for $i, j = 1, 2$ and $i \neq j$,

$$F_i^\alpha = \frac{1}{3}\frac{\Lambda}{Y_0}\Big\{\Gamma_i^\alpha\,(2\sigma_i^\alpha - \sigma_j^\alpha) + \tfrac{1}{3}\Gamma_j^\alpha\big[\,2(\sigma_{i1}^\alpha)^2 - 2\,\sigma_i^\alpha\sigma_j^\alpha - (\sigma_j^\alpha)^2\big]\Big\}. \tag{5}$$

Here $\bar{\sigma} = [(\sigma_1)^2 + (\sigma_2)^2 - \sigma_1\sigma_2]^{1/2}$, where σ_1 and σ_2 are the Cauchy stress components. Appropriate boundary conditions express equality of overall forces normal to the groove direction and equality of total strains in the groove direction. Consider now the two stress histories shown on figure 2.2 defined by a proportional path OAC ($\sigma_2 = m_0\,\sigma_1$) and some nonproportional path OACD with break point position $k \quad \in [0,1]$. Let the speed $\dot{\sigma}$ of the representative point in such a stress space take the values from 15 MPa/s (low strain rate) to 1900 MPa/s (medium strain rate). Results of integration of governing

Figure 2: Stress histories

differential equations are visualized for "medium strain rate" on two figures for nonproportional path with stress direction $m_0 = 0.6$ and $k = 0.6$. Figure 3 shows Forming Limit Diagrams for diverse $f_0 = t_B/t_A$. The diagrams describe σ_1/Y_0 versus ε_1 outside the groove (dotted line) as well as in the groove (continuous lines). In order to show the influence of stress direction and nonproportionality, figure 3b shows ε_2 as functions of ε_1 for a fixed thinning parameter f_0.

3   Mesoscopic model of sheet deformation

Now, a deformed sheet element is considered as a polycrystalline aggregate. To describe the behavior of single grain with M slip systems the regularized Schmid law is used. It creates a smooth, but strongly non-linear yield surface with rounded-off corners [8]. The corresponding yield surface of a polycrystalline element is given by the $2\,\tilde{n}$-th order polynomial [11]. The above yield
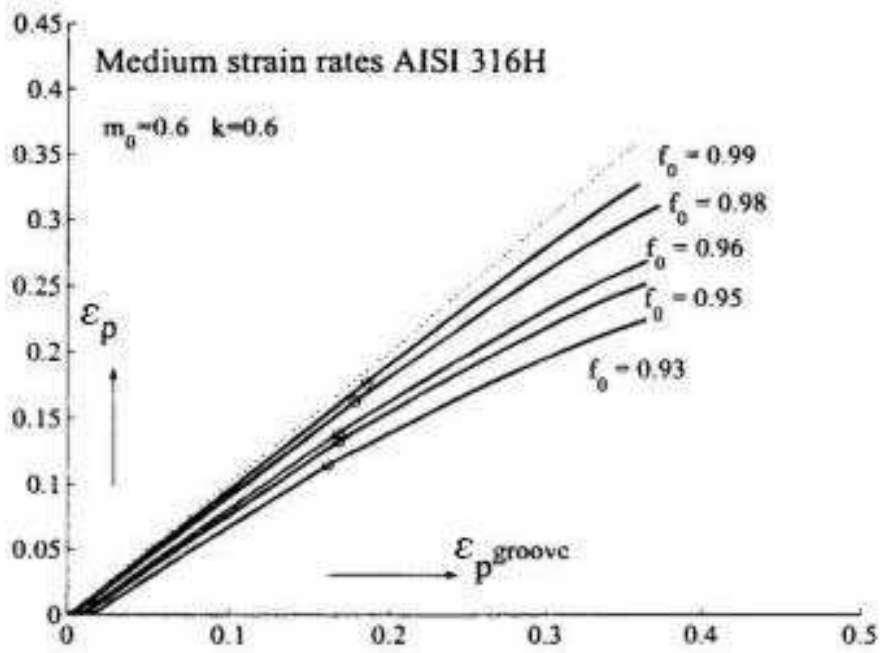
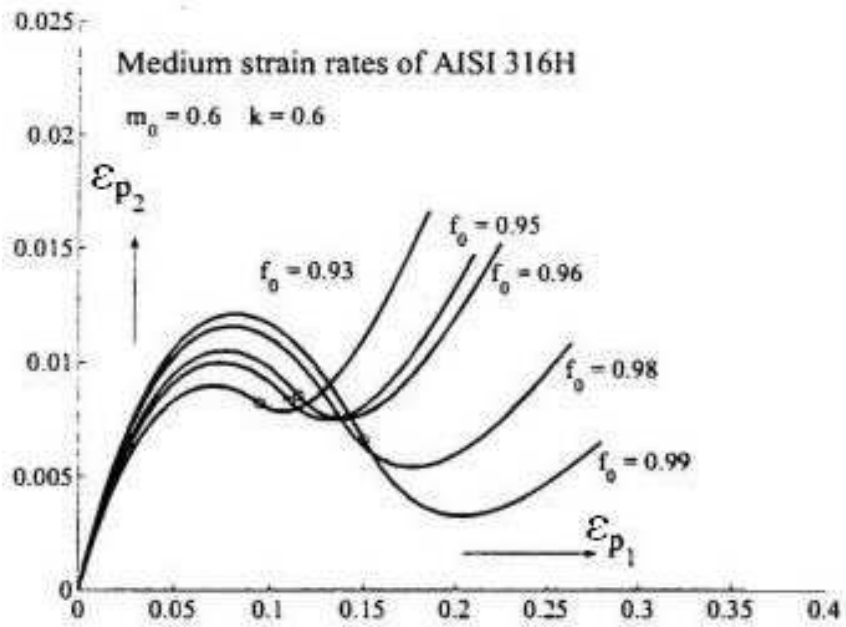Figure 3a: Forming Limit Diagrams at "medium strain rate"

Figure 3b: Strain components in the groove at "medium strain rate"

surfaces are described by the following two equations:

$$\sum_{r=1}^{M} \left(\frac{\tau^{(r)}}{\tau_{cr}^{(r)}}\right)^{2n} = m \quad and \quad \sum_{g=1}^{N} \frac{\gamma^g}{m^g} \sum_{r=1}^{M} \left(\frac{\tau^{(r,g)}}{\bar{\tau}_{cr}^{(r,g)}}\right)^{2\tilde{n}} = \tau_{cr}^{2\tilde{n}}. \tag{6}$$

In the first equation: $\tau^{(r)}$ is the resolved shear stress on the r-th slip system, $\tau_{cr}^{(r)}$ — its critical value and $m > 0$ as well as $1 \leqslant n \leqslant 20$ are non-dimensional material constants of the considered grain. In the second equation g is grain number and γ^g — volumetric ratio of g-grains.

The flow rule and plastic spin rule conjugated with the regularized Schmid law enable to watch the stress state and the lattice rotation in each grain of polycrystalline element.
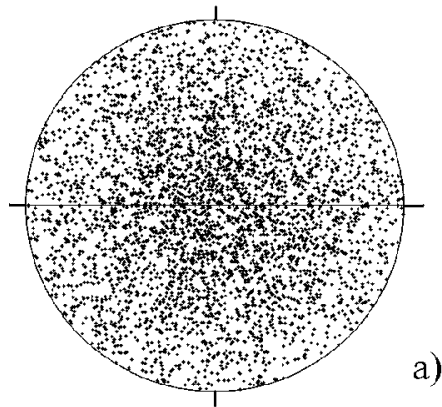
In this way, one can observe - on the mesoscopic level - the texture development caused by the plastic deformation of the polycrystalline element. Assume 1000 f.c.c. grains in the considered polycrystalline element. For $f_0 = t_B/t_A$ =0.96 and nonproportional loading with $m_0 = 1$ and k = 0.2 (see figure 2.2), we obtain the pole figures shown in figure 4.

On the other hand, changes of the macroscopic yield surface and development of plastic anisotropy in the element can be observed. Particularly, one can investigate the evolution of the ratio of the plastic strain and plastic strain rate components (figures 4 and 6).
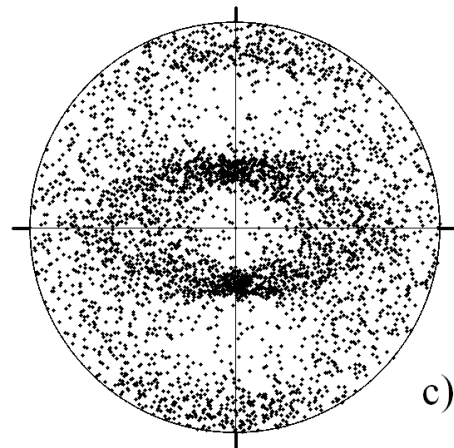
4   Conclusions

The technologically important problem of strain localization in thin sheets is treated by a tensor representation of viscoplastic evolution equations. The results are presented by the Forming Limit Diagrams giving simple and direct information of limit strains location. Analysis of the metal behavior on the mesoscopic level gives new opportunities. In particular, it is expected that using the polycrystalline yield surface generated by the developed texture,as proposed in the present paper, will improve the predictions of the FLDs based on purely phenomenological models.
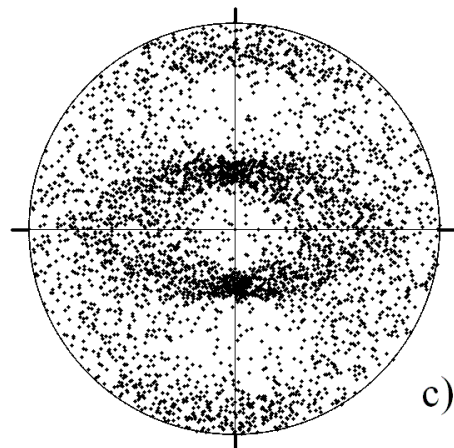
(a) Initial

(b) Outside of groove

(c) In the groove

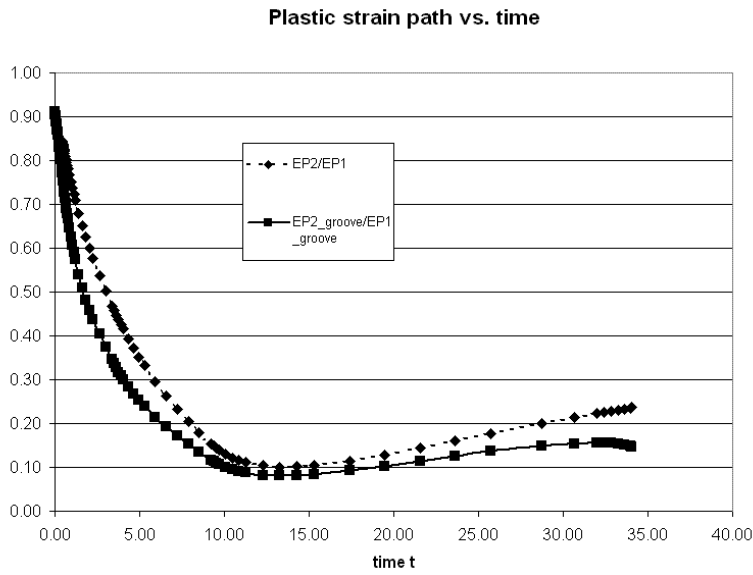Figure 4: Pole figures $< 111 >$ for nonproportional ($m_0 = 1, k = 0.2$) loading

Plastic strain path vs. time

Figure 5: Evolution of the ratio $\varepsilon_{P2}/\varepsilon_{P1}$ for nonproportional loading ($m_0 = 1$, $k = 0.2$)

Plastic strain rate path vs. time
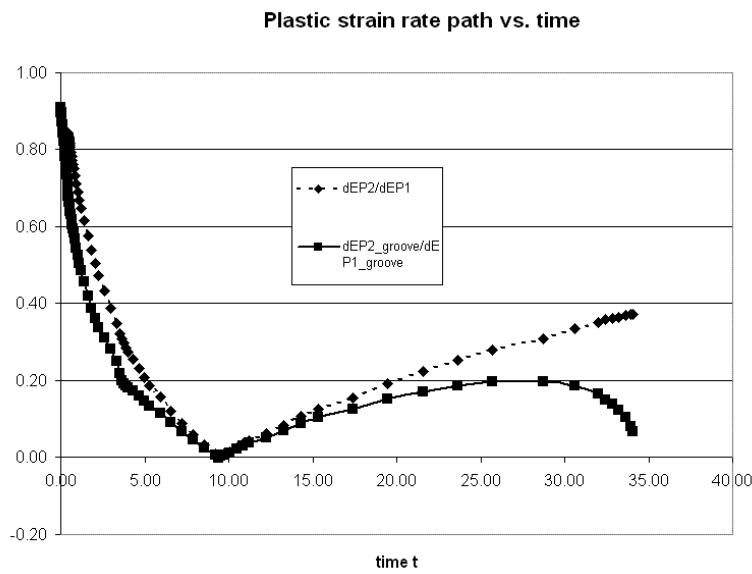

Figure 6: Evolution of the ratio $\mathrm{d}\varepsilon_{P2}/\mathrm{d}\varepsilon_{P1}$ for nonproportional loading ($m_0 = 1$, $k = 0.2$)

References

[1] P. Perzyna, Fundamental Problems in Viscoplasticity, *Advances in Applied Mechanics* **11** (1971) 313-387.

[2] J. L. Chaboche and G. Rousselier, On the plastic and viscoplastic constitutive equations, *Trans. ASME, PVT*, **105** (1983) 153-164.

[3] Yu. N. Rabotnov, *Elements of Hereditary Solids Mechanics*, Mir Publishers, Moscow (1980).

[4] M. Micunovic, C. Albertini and M. Montagnani, High strain rate viscoplasticity of AISI 316 stainless steel from tension and shear experiments, In: *Solid Mechanics*, eds, P. Miljanic, Serbian Acad. Sci.-Sci. Meetings **87**, Dept. Techn. Sci. **3** (1997) 97-106.

[5] C. Albertini, L. J. Griffits, M. Montagnani, A. Rodis, P. Mariotti, A. Paluffi and G. Pazienza, Material characterization by an innovative biaxial shear experiment at very large strain rates, *Journal de Physique IV* 1 (1991) C3 435-C3 440.

[6] M. Micunovic, Multiaxial dynamic experiments and viscoplasticity of metals, *Scientific Review* **16** (1-22) 1996.

[7] Z. Marciniak and K. Kuczynski, Limit strains in the process of stretch forming sheet metal, Int. J. Mech. Sciences 9/9 (1967) 609-620.

[8] W. Gambin, Crystal plasticity with rounded-off corners, *ZAMM* **71**, 4 (1991) T 265-T 268.

[9] W. Gambin, Refined analysis of elastic-plastic crystals, *Int. J. Solids Structures* **29**, 16 (1992) 2013-2021.

[10] W. Gambin, *Plasticity and Textures*, Kluwer Academic Publishers, Dordrecht (2001).

[11] K. Kowalczyk, Evolution of plastic anisotropy of the polycrystalline materials in large deformation processes, *Engng Trans.* **49**, 4 (2001) 537-571.

[12] K. Kowalczyk and W. Gambin, Model of plastic anisotropy evolution with texture-dependent yield surface, *Int. J. Plasticity* **20** (2004) 19-54.

Dvoskalni pristup otkazu usled dinamičke lokalizacije ploče od AISI *316H* nerdjajućeg čelika

Otkaz usled dinamičke lokalizacije ploče od AISI $316H$ nerdjajućeg čelika za proporcionalne i neproporcionalne naponske istorije se posmatra na makroskopskom i mezoskopskom nivou. Na makroskopskom nivou predlažemo: (1) zamenu vremena kao nezavisne promenljive jednom funkcijom plastične disipacije i (2) zavisnošću početnog ekvivalentnog napona tečenja od brzine promene napona.

S druge strane, na mezoskopskom nivou uvodimo regularizovani model Schmid-a za opis ponašanja posebnih zrna. Pritom se površ tečenja polikristala generiše razvojem teksture što omogućava poboljšanje dijagrama granične deformabilnosti za element ploče.